Mapping relative extinction risk for biodiversity conservation

Article *in* Biological Conservation · October 2018

DOI: 10.1016/j.biocon.2018.07.012

Xinghua Sui
Sun Yat-Sen University

Biological Conservation 226 (2018) 168–176

Contents lists available at ScienceDirect

Biological Conservation

journal homepage: www.elsevier.com/locate/biocon

Mapping relative extinction risk for biodiversity conservation

Xinghua Sui[a,*], Lingfeng Mao[b], Ying Liu[a], Fangliang He[c,d,**]

[a] State Key Laboratory of Biocontrol, School of Life Sciences, Sun Yat-sen University, Guangzhou 510275, China
[b] College of Biology and the Environment, Nanjing Forestry University, Nanjing 210037, China
[c] ECNU-Alberta Joint Lab for Biodiversity Study, East China Normal University, Shanghai 200062, China
[d] Department of Renewable Resources, University of Alberta, 114 St.-89 Ave., Edmonton, Alberta T6G 2H1, Canada

1. Introduction

Biodiversity mapping (i.e., presenting and analyzing the distribution of biodiversity in space) is an essential tool in biogeography and conservation biology (Brooks et al., 2006; Pimm et al., 2014). An important application of biodiversity maps is their use in modeling the geographical distribution of extinction risk of species to understand the underlying causes of the risk and to allocate conservation priorities (Davies et al., 2006). Biodiversity mapping is particularly powerful if it is used in combination with other well-established conservation assessment systems such as the International Union for Conservation of Nature (IUCN) Red List (IUCN, 2001). The IUCN addresses species endangerment by establishing quantitative criteria for assessing extinction risk at the regional or global scale. With this species-specific knowledge on extinction risk, threatened species can be directly mapped to identify hotspots of extinction risk (Brooks et al., 2006). Depending on the specific conservation targets, conservation hotspots can also be delineated using combined measures of species diversity (usually overall or small-ranged species richness), ecosystem services (e.g., forest carbon stocks) and extrinsic threats (as measured by indexes of human presence or land cover change) (Myers et al., 2000; Jenkins et al., 2013). Ideally, high congruence among these measures would provide a “silver bullet” for multiple facets of biodiversity conservation or co-benefits for climate change mitigation (Canadell and Raupach, 2008).

However, incongruence between the hotspots defined by different measures (e.g., total species richness versus threatened species) is frequently reported (Orme et al., 2005; Grenyer et al., 2006). The spatial incongruence between those mapped “hotspots” suggests that different mechanisms may underlie spatial distribution of species richness, restricted-range species, and threatened species. It is well recognized that broad-scale patterns of species richness are strongly influenced by widespread species rather than rare species (Lennon et al., 2004). Compared with widespread species, range-limited (e.g., < 250,000 km^2; hereafter termed "endemic") species are more concentrated in areas featuring a high environmental variation, rare/unusual climate (Ohlemüller et al., 2008), or historically stable climate (Sandel et al., 2011). Because of the limited distribution or rarity in number, endemic or rare species are particularly vulnerable to anthropogenic disturbances such as destruction and fragmentation of natural habitats (Fahrig, 2003). As such, an area with more endemic species tends to be an extinction hotspot, which is traditionally delineated by the total number of threatened species (Brooks et al., 2002).

A potential problem with conventional biodiversity mapping based on the absolute number of threatened species is that this cannot adequately inform the degree of threat, i.e., "vulnerability" (Margules and Pressey, 2000) in mapped areas. Although using absolute species richness has the advantage of highlighting particularly biodiverse regions at risk, it may overlook less diverse areas with considerable threats, for instance, many populous regions in eastern China could nevertheless lose valuable local biodiversity and ecosystem functioning if land use transformation continues to occur. This problem is commonly dealt with by dividing the number of threatened species (denoted as TSR) by the total number of species (denoted as SR) and then mapping the ratio (Davies et al., 2006; Lee and Jetz, 2011). However, the TSR/SR ratio (also termed *crude rate* in epidemiology studies) is not suitable for mapping risk because the variance of this ratio depends on the size of the denominator (i.e., SR) in each mapping unit. Specifically, given an independent risk π of being exposed to an event for a given number of species (SR), the number of species observed to be threatened (TSR) can be taken to follow a binomial distribution. The variance of the TSR/SR ratio estimator is $\pi(1-\pi)/SR$. If SR is small, the variance in the ratio is high; if SR is large, the variance in the ratio is low. In other words, the smaller SR, the less precise the ratio will be as an estimator of π. Hence, the appearance of a large ratio could be entirely or partly due to the small number problem (Elliott and Wartenberg, 2004), and the resulting ratios will be highly variable and difficult to compare. Consequently, any ratio map suggesting "outliers" may be spurious, as the extreme values may simply result from high variability of the estimate.

To map the risk of species extinction, it is necessary to compare the ratio to a benchmark. In other words, the observed number of threatened species must be compared to an expected number of threatened species to correctly represent the degree of extinction risk.

---

* Corresponding author.
** Correspondence to: F. He, Department of Renewable Resources, University of Alberta, Edmonton, Alberta, T6G 2H1, Canada.
E-mail addresses: suixingh@mail.sysu.edu.cn (X. Sui), fhe@ualberta.ca (F. He).

https://doi.org/10.1016/j.biocon.2018.07.012
Received 30 January 2018; Received in revised form 4 July 2018; Accepted 15 July 2018

Furthermore, smoothing techniques such as Bayesian smoothers (Clayton and Kaldor, 1987) are required to address variance instability in ratios due to the variability of SR across spatial units.

Here, we propose "relative extinction risk" (RER) to quantify geographic variation in extinction (or threatened) risk. The concept of RER was initially developed and widely used in epidemiology for mapping disease distribution and outbreak (Sartorius et al., 2013; Saint-Jacques et al., 2016), or identifying and predicting high-risk areas (Devine et al., 1996; Shacham et al., 2017). For example, Shearer et al. (2018) assembled 1155 geographical records of yellow fever virus infection and incorporated environmental and biological explanatory covariates to map and predict the incidence and the relative risk of apparent yellow fever virus infection across the Americas and Africa. In our study, "threatened species" is analogous to "incidence of disease" in epidemiology (Wakefield, 2007; Lawson, 2013). Following this concept, RER is measured as the ratio of the number of observed threatened species to the expected number of threatened species. A relative extinction risk significantly higher than one indicates that the region is suffering from an excessively high level of extinction threats. In turn, such high proportions of local loss of species may risk ecological functioning or biological insurance (Hooper et al., 2012). Mapping relative extinction risk thus provides valuable information for identifying areas in need of immediate conservation action. Furthermore, the resulting estimate of relative extinction risk provides a natural means to model the effect of potential threatening factors on extinction risk, as is used in epidemiology and public health studies (Sartorius et al., 2011; Lawson, 2013).

In this study, we mapped and compared relative extinction risk distribution for threatened angiosperm species in China to demonstrate the capacity of this method. We consider China as a particularly relevant country for mapping threatened species as China is one of the megadiverse countries (~35,000 seed plant species) and has suffered serious environmental problems that threaten the survival of many species (He, 2009). We compiled an extensive database on the taxonomy, distribution, environmental, and human activity factors for the Red List angiosperm species in China to address the following three questions: (1) Are the hotspots of species richness, threatened species, and relative extinction risk spatially congruent? (2) Are the spatial patterns of threatened species richness and relative extinction risk explained by the same set of environmental and human activity risk factors? (3) How may the degree of plant extinction risk affect local ecosystem functioning (as measured by net primary productivity) and which of the extinction risks (TSR versus RER) better reflects the degeneration of ecosystem functioning? To answer these questions, we mapped and compared the distributions of threatened species and the relative species extinction risk. We then modeled the effects of environment and human activities on the distributions of threatened species and relative extinction risk. We further examined the correlation of threatened species richness and relative extinction risk with net primary productivity (NPP). We concluded the study by discussing the implications of RER methodology for informing conservation practice.

2. Study data

2.1. Data on IUCN Red List plant species

For the ease of description of the mapping method, we first introduce the data on threatened species in China and the related covariates. The latest (2013) China IUCN Red List species (http://www.mep.gov.cn/gkml/hbb/bgg/201309/W020130912562095920726.pdf) were used in this study. This Red List evaluated 29,530 higher plant species and infraspecific taxa in 2793 genera and 249 families, of which 17,701 are endemic in China. Based on the criteria of IUCN, species are placed into one of seven categories: least concern (LC), near-threatened (NT), vulnerable (VU), endangered (EN), critically endangered (CR), extinct in the wild (EW), and extinct (EX), with those in the categories CR, EN, or VU classified as Threatened. After screening species' names with the latest version of *Flora of China* (http://www.efloras.org/flora_page.aspx?flora_id=2) to exclude synonyms, we identified 27,399 angiosperm species with 925,195 spatial distribution records from the county-level Chinese Vascular Plant Distribution Database (CVPDD), which was compiled from three sources of data: *Flora Reipublicae Popularis Sinicae* (http://frps.eflora.cn/), provincial and regional floras in China (http://www.metasequoia.org/local.htm). We further retrieved and georeferenced 9,166,930 plant specimen records from National Specimen Information Infrastructure (http://www.nsii.org.cn; accessed in September 2017). The taxonomy of the specimen records was checked with a name checking service (http://www.nsii.org.cn/2017/namesautocheck.php) to ensure they were comparable with *Flora of China*, Species2000 (Checklist 2017, http://www.sp2000.org.cn/2017), and the CVPDD. The full list of Chinese angiosperm species and their range sizes are included in the Appendix (Table S1). Considering the dramatic changes in human activities in China in recent decades, we used 1,903,030 records with valid county-level distribution since the 1980s to correct the distribution information of the CVPDD. We repeated the analyses using 4,550,638 records since the 1950s to evaluate the influence of sampling bias of specimen collection on the quality of distribution data (Yang et al., 2013). We found the results were similar between the two datasets, so we only reported the results with specimen information correction since the 1980s in the main text but presented the results with datasets since the 1950s in Appendix Table S2.

To eliminate the influence of county area on the estimation of species richness (Rosenzweig, 1995), we gridded species distribution data and all the environmental and human activity variables (see below) to a 50 km scale with equal area projection. We excluded the grid cells on borders or coasts that had less than half of their area on land or inside China. The grids in Hainan and Taiwan islands were excluded. Finally, 3769 grid cells were used in this study. The number of threatened species in each grid cell was the number of IUCN threatened species, and the relative extinction risk was calculated accordingly following methods described in the section "Modeling relative extinction risk" below. To identify risk factors, the distributions of the threatened species richness and the relative extinction risk were modeled using environmental, human activity, and spatial variables as described below. We repeated the above analyses using 100 km grid cells to further evaluate the robustness of our results to different spatial scales and the transformation from county-level polygons to gridded distributions. We found that the results were mostly consistent with those using 50 km grid cells. Therefore, we reported only the results for 50 km grid cells in the main text but included the 100 km grid results in the Appendix (Fig. S1 and Table S3).

2.2. Environmental variables (ENV)

Environmental variables include the bioclimatic variables extracted from the WorldClim Database (grid size: 30 s, ~1 km) (Hijmans et al., 2005) and the annual actual evapotranspiration (AET) and annual potential evapotranspiration (PET) data compiled from the Global Evapotranspiration and Water Balance Data Sets (Ahn and Tateishi, 1994). These variables were grouped into 4 categories: (1) Energy factors, including mean annual temperature (MAT), mean temperature of the coldest month (TCM), mean temperature of coldest quarter (TCQ), and PET; (2) water availability factors, including mean annual precipitation (MAP), mean precipitation of the driest month (PDM), AET, and moisture index (MI) (calculated as AET / PET) (Shafer et al., 2001); (3) heterogeneity factors, including the range of MAT, MAP, and standard deviation of altitude within each grid; (4) climatic seasonality factors, including temperature seasonality (TS) and precipitation seasonality (PS).

To quantify the availability of analogous climates (AAC) for species migration, we calculated the average Euclidian distance in climatic space between each focal cell and all other cells within 500 km. The climatic space was defined with the first two principal component axes (PCA) which captured 79.3% of the variation in the above 13 environmental variables after excluding variables having pairwise Pearson correlation coefficient > 0.9. Areas with high AAC values have more similar climatic conditions amenable to dispersal or migration.

Following Sandel et al. (2011), long-term climate stability was represented by Late Quaternary climate-change velocity (CCV), measured as the mean annual temperature velocity since the Last Glacial Maximum (21,000 years ago). CCV was calculated by dividing the temperature change over time by the local temperature change across space, as an indication of the dispersal rates required to track suitable climates across the surrounding topography. The past mean annual temperature was calculated using the mean value of the CCSM3 and MIROC3.2 simulations from the Paleoclimate Modelling Intercomparison Project Phase II.

2.3. Human activity and land fragmentation variables (HAL)

Ground validated land cover/land use data with 15 land use types (Appendix Table S4) were compiled from Ran et al. (2010), comprising percentage area covered by corresponding vegetation types at the original 1 km resolution that was aggregated to 50 × 50 km equal area projected grids to match the species distribution maps. Historical habitat loss (before 2000) in China was estimated as the sum of land area occupied by urban settlements, crops, and two thirds of pasture area, under the assumption that pasture lands were incompletely cultivated and less intensively used than croplands or urban areas (Lee and Jetz, 2011). Recent habitat loss (2000–2015) was aggregated and projected from forest cover data at 30-meter resolution (Hansen et al., 2013). The final habitat loss (HL) was the sum of historical and recent habitat loss. We compiled data on population density (POP) in 2010 (http://sedac.ciesin.columbia.edu/data/collection/gpw-v3) and road length (RL) from 1980 to 2010 (http://sedac.ciesin.columbia.edu/data/set/groads-global-roads-open-access-v1) as surrogate measures of land use intensity. We also compiled data from Global Human Footprint in 2009 (Venter et al., 2016) as a composite measure of human pressure suggested by previous studies (Di Marco et al., 2013).

We calculated landscape fragmentation metrics for each 50 km grid by batch processing original 1 km land use maps; they included patch clumpy index (CLUMPY), and core area index (CAI_MN). We used a binary classification of habitat/non-habitat, which combined natural land cover types into a single habitat class. Shannon's Diversity Index (SHDI) and Shannon's evenness index (SHEI) were calculated for all 15 land use types as landscape level measures of habitat fragmentation (Wang et al., 2014).

2.4. Spatial variables (SEF)

Moran's *I* test was performed to check for spatial autocorrelation in the distribution of the threatened species richness (TSR) and the relative extinction risk (RER). We then included spatial eigenvector mapping (Griffith and Peres-Neto, 2006) together with the above environmental and human activity variables in the regression models of TSR and RER to account for the possible spatial autocorrelation in TSR and RER. We selected spatial eigenvector filters with a forward selection procedure and stopped including further eigenvector filters into the models of TSR and RER once the Moran's *I* values in the residuals of the regression models were no longer significant (Griffith, 2003).

2.5. Relationships between different measures of extinction risks and ecosystem functioning

We made an attempt to link extinction risks with ecosystem functioning. We used net primary productivity (NPP) to measure ecosystem functioning. The Moderate Resolution Imaging Spectroradiometer (MODIS) gridded 1 km annual NPP was derived from satellite measures of vegetated cover and density from 2000 to 2015 (Zhao and Running, 2010). We mapped and masked the original data to exclude cropland and urban settlements. Temporal change in NPP at each grid was characterized by the slope of the linear trend with respect to time (2000–2015). Relative temporal change of NPP was calculated as the slope of the linear regression line divided by NPP in 2000 to measure degeneration of ecosystem functioning over time among areas.

3. Modeling relative extinction risk

3.1. Extinction risk mapping

We mapped threatened species richness (TSR) and relative extinction risk (RER), respectively, and compared the difference between the two mapping methods. For the traditional mapping, the total species richness (or the threatened species richness) is directly placed on maps. The biodiversity (or the threat) hotspots are then delineated as those cells ranked in the top 2.5% or 5% by the number of (threatened) species (Ceballos and Ehrlich, 2006).

In the context of extinction risk mapping, the threatened species richness (TSR_i) in a spatial unit *i* is assumed to follow a Poisson distribution with mean (and variance) $\theta_i E_{TSR,i}$, where $E_{TSR,i}$ is the expected number of threatened species, and θ_i is the relative extinction risk in a spatial unit *i*. More precisely, the distribution of TSR_i is conditional on the unknown relative risk parameter θ_i

$$TSR_i|\theta_i \sim \text{Poisson}(\theta_i \cdot E_{TSR,i}). \tag{1}$$

The maximum likelihood estimator for the relative extinction risk (θ_i) follows as:

$$\hat{\theta}_i = \frac{TSR_i}{E_{TSR,i}}, \tag{2}$$

with variance:

$$Var[\hat{\theta}_i] = \frac{\theta_i}{E_{TSR,i}}. \tag{3}$$

Note that the expected number of threatened species is computed by applying a reference estimate for the risk (r_+) to the total (threatened + unthreatened) species richness in unit *i* (SR_i):

$$E_{TSR,i} = SR_i \cdot r_+, \tag{4}$$

where the overall mean risk r_+ is obtained from the marginal distribution of the observed events TSR_i, calculated as the ratio of the total threatened species richness (TSR_+) to the total species richness (SR_+) of the study area (the subscript + indicates the sum over all the spatial units):

$$r_+ = \frac{TSR_+}{SR_+}. \tag{5}$$

As $E_{TSR,i}$ depends on the population at risk (SR_i, i.e., the total species richness in area *i*), the variance of the estimate $\hat{\theta}_i$ will vary with SR_i. To correct for variance instability, an empirical Bayes (EB) smoother is widely applied by shrinking the estimates of $\hat{\theta}_i$ in each area towards the overall mean risk as an inverse function of the inherent variance (Clayton and Kaldor, 1987). In Bayesian statistics, the overall mean risk r_+ is a prior, which is conceptualized as a random variable with its own "prior" distribution. Specifically, assuming the prior distribution of θ_i to have mean μ_i and variance σ_i^2, the best linear Bayes estimator of the RER is obtained by (Clayton and Kaldor, 1987)

$$\hat{\theta}_i^{EB} = \omega_i \hat{\theta}_i + (1 - \omega_i)\mu_i, \tag{6}$$

with weights ω_i

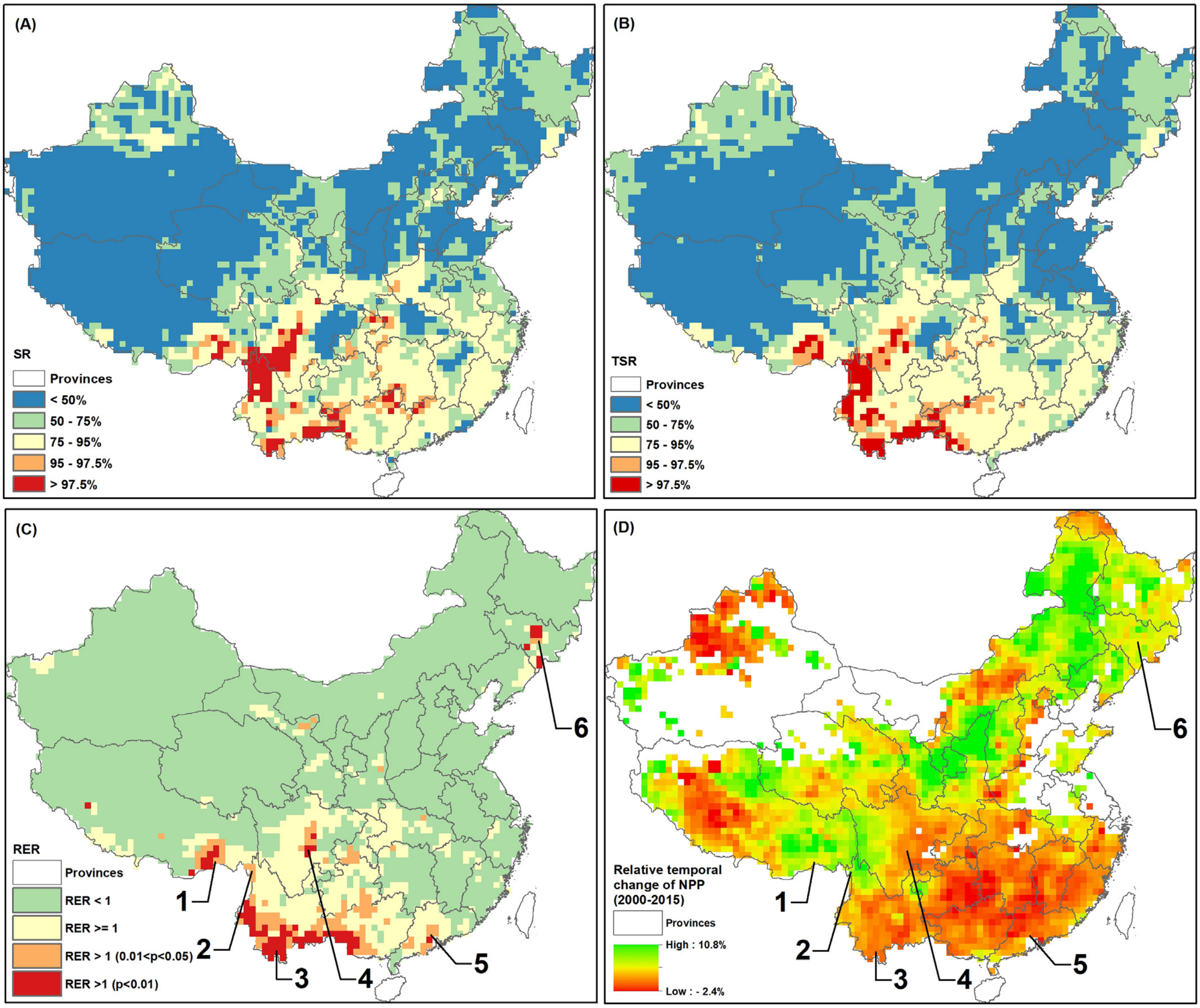

Fig. 1. (A) Distribution of angiosperm species in China at 50 × 50 km resolution, showing species richness (SR), (B) threatened species richness (TSR), which varies from zero to 761, (C) the relative extinction risk (RER), and (D) relative temporal change of NPP during 2000–2015 (calculated as the temporal NPP change divided by the NPP in year 2000). The SR and TSR hotspots (in panel A and B) with the upper 2.5% and 5% quantiles are shown in red and orange, respectively. In panel C, the red and orange colors indicate RER hotspots at the significance levels $P < 0.01$ and $P < 0.05$, respectively. The numbers in panels C and D indicate Southeast Tibet (area 1), Hengduan Mountains (area 2), Xishuangbanna Region (area 3), Sichuan Basin and Chengdu Plain (area 4), Guangdong Hills (area 5), and Northeast Plain (area 6). (For interpretation of the references to color in this figure legend, the reader is referred to the web version of this article.)

$$\omega_i = \frac{\sigma_i^2}{\sigma_i^2 + (\mu_i/E_{TSR,i})}, \tag{7}$$

and variance

$$Var[\hat{\theta}_i^{EB}] = \sigma_i^2 + (\mu_i/E_{TSR,i}). \tag{8}$$

The EB estimate of RER is thus a weighted average of $\hat{\theta}_i$ and the "prior" with weights inversely related to their variance. Weight ω_i approaches one when $E_{TSR,i}$ is large, giving all the weight in Eq. (6) to the original estimate $\hat{\theta}_i$. As $E_{TSR,i}$ becomes smaller, and thus the variance of the original estimate increases, more weight is given to the prior overall mean risk r_+.

Here we adopt a multivariate log-normal distribution for θ_i:

$$\log(\theta_i) = \lambda_i, \tag{9}$$

with

$$\lambda \sim MVN(\mu, \Sigma), \tag{10}$$

where λ is an N by 1 vector of λ_i, μ is a vector of prior means, and Σ is a variance-covariance matrix. Estimation of the log-relative risk $\hat{\lambda}_i$ is not taken as $\log(TSR_i / E_{TSR,i})$ but $\log((TSR_i + 0.5) / E_{TSR,i})$, because the former is not defined when TSR_i is zero. In the simple case with an i.i.d. prior $N(\mu, \sigma^2)$, the expectation–maximization (EM) algorithm can be used to obtain estimates of the mean and variance of the normal distribution Eq. (10) by successively updating the following EB estimator of λ_i until convergence (Lawson, 2013):

$$\log(\hat{\theta}_i^{EB}) = \hat{\lambda}_i^{EB} = \frac{\hat{\phi} + \hat{\sigma}^2(TSR_i + 0.5)\hat{\lambda}_i - 0.5\cdot\hat{\sigma}^2}{1 + (TSR_i + 0.5)\hat{\sigma}^2}, \tag{11}$$

where prior estimates of the mean and variance are given by

$$\hat{\phi} = \frac{1}{n}\sum_{i=1}^{n}\lambda_i = \bar{\lambda}, \tag{12}$$

and

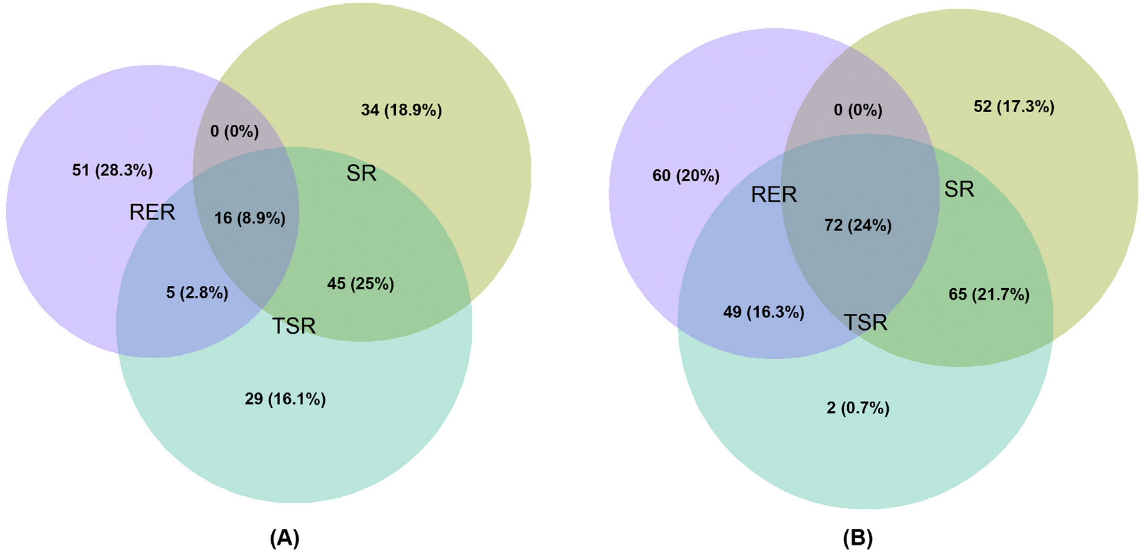

Fig. 2. Venn diagram showing the number and percentage of hotspots that are spatially overlapped among the three diversity components: species richness (SR), threatened species richness (TSR), and relative extinction risk (RER). (A) SR and TSR hotspots are identified by the grid cells of the 2.5% upper quantile while RER hotspots are defined at $P < 0.01$; (B) SR and TSR hotspots are the 5% upper quantile while RER hotspots are defined at $P < 0.05$.

$$\hat{\sigma}^2 = \frac{1}{n}\left\{\hat{\sigma}^2\sum_{i=1}^{n}[1+\hat{\sigma}^2(TSR_i+0.5)]^{-1} + \sum_{i=1}^{n}(\lambda_i-\hat{\phi})^2\right\}. \tag{13}$$

Following the above assumptions, “relative extinction risk hotspots” can be naturally defined via the probability map of the log-normal distribution (Lawson, 2013). A cell is an RER hotspot if the observed threatened species richness is significantly higher than expected under the log-normal model at $P \le 0.05$.

Spatial congruence among the three types of hotspots (total richness, the number of threatened species, and relative extinction risk) was evaluated by calculating the degree of spatial overlap and the correlations between them.

3.2. *Modeling extinction risk in terms of environmental, human activity, and spatial covariates*

We used log-transformed threatened species richness as the response variable in the following analysis. This log-linear regression model is commonly used to model species richness (e.g., Ricklefs and He, 2016). For the relative extinction risk θ_i (Eq. (9)), log-transformed θ_i has the property that it is centered at 0 with equal ranges on either side (Prentice, 1985); the prior (Eq. (10)) also provides a natural means to introduce explanatory variables in the log-linear model (Lawson, 2013):

$$\log(\theta) = \alpha_0 + \alpha\log(SR) + \beta\times\mathbf{ENV} + \gamma\times\mathbf{HAL} + \delta\times\mathbf{SEF} + \varepsilon, \tag{14}$$

where ε is a non-spatial random error term. The response variable θ can be TSR or RER. Environment (ENV), human activity (HAL) variables, and the selected spatial eigenvector filters (SEF) were included in the model to determine their effects on TSR and RER. For both TSR and RER models, log-transformed total species richness (SR) was included to account for the background species pool.

3.3. *Model selection*

Multicollinearity in the ENV and HAL variables was removed by excluding those variables with correlation coefficient > 0.9. The selected explanatory variables were included in the regression model (14). For human activity variables (HAL), the quadratic term of the habitat loss area was included to account for the possible quadratic effect. Interaction terms between habitat loss (HL), and habitat diversity (SHEI), land use intensity (population density and road length), and fragmentation metrics (CAI_MN) were also included to account for potential interactive effects between anthropogenic threats.

Model selection was based on the Akaike information criterion (AIC). The relative importance of the selected variables was assessed using the probability of each variable being included in the “best” models, estimated by summing the Akaike's weights of all candidate models where the variable was included. Model fit was evaluated using adjusted R^2_{adj} and AIC. All numeric variables were standardized to 0–1 by $(x - x_{\min}) / (x_{\max} - x_{\min})$ to facilitate comparison of the estimated coefficients.

Landscape fragmentation metrics were calculated using FRAGSTATS (version 4.2) (McGarigal et al., 2012). Empirical Bayes estimates of smoothed relative risk were implemented in the R package “DCluster”. Moran's I values and tests were computed with the R package “spdep”. Model selection and inference were implemented with the R package “MuMIn”. All statistical analyses were performed using R (https://www.r-project.org/) and ArcGIS 10.1 (Environmental Systems Research Institute (ESRI), Redlands, CA.).

4. Results

The total species richness (SR), threatened species richness (TSR), and relative extinction risk (RER) were unevenly distributed across China (Fig. 1). High total and threatened species richness were concentrated in the same mountainous areas in southwestern and central China (Fig. 1A, B; see areas 1, 2, and 3 in Fig. 1C). Species richness alone explained 66% of the variation in TSR, indicating the high spatial congruence between SR and TSR. In contrast, only 18% of the variation in RER was explained by SR after spatial dependence was accounted for. The distribution of high RER is less concentrated but high RER mostly distributed in southeast Tibet (area 1) and southwestern China (area 2 and 3), with some sparsely scattered in other parts of China, including the Sichuan Basin, Guangdong Hills and Northeast Plain (areas 4, 5, and 6 in Fig. 1C).

The spatial incongruence between RER and SR was also reflected in the spatial overlap of their hotspots. Under the 2.5% upper quantile criterion for SR and TSR and $P < 0.01$ significance level for RER, only 16 cells (40,000 km^2) contained overlapping RER and SR hotspots (Fig. 2A), which account for 22.2% of the total 72 RER hotspot cells (180,000 km^2). In contrast, TSR and SR shared 61 hotspot cells

Table 1

The best models for threatened species richness and relative extinction risk selected for environmental (ENV), human activity and landscape (HAL), and spatial (SEF) variables. The adjusted R^2 was used to evaluate the overall goodness of fit. *** indicates $P < 0.001$, ** $P < 0.01$, * $P < 0.05$. Variables that were not selected are denoted by "-". Variables that were selected but not significant are not asterisked. Note that the relative extinction risk and the total and threatened species richness are all log-transformed in the regression models.

Variables	Threatened species richness	Relative extinction risk
(Intercept)	−3.13***	−0.51***
SR	0.92***	0.01
Energy and water availability		
PET	1.06***	0.47***
MI	0.32***	0.22***
PCQ	−1.58***	−0.39***
Topography and heterogeneity		
ALT	−0.06	−0.31 ***
ALT_STD	-	0.2 ***
Climatic variability/stability		
MDR	−0.92***	−0.39***
CCV_MN	−0.75***	−0.36***
AAC	−0.84***	−0.45***
PS	−0.47***	−0.19***
Habitat loss		
HL	−0.27***	0.12
HL^2	-	−0.43***
Land use intensity		
HFP	0.48***	0.31***
RL	-	0.06**
POP	1.61***	0.48***
POP^2	1.46**	-
Habitat fragmentation		
SHEI	0.22***	0.15***
CAI_MN	−0.04	0.02***
Interactions		
HL * POP	−3.94***	-
HL * CAI_MN	2.13***	-
HL * CAI_CV	0.45***	0.28***
R^2_{adj}	0.93	0.79

Note: Covariate abbreviations are as follows: SR: total species richness, PET: annual potential evapotranspiration, MI: moisture index, PCQ: mean precipitation of the coldest quarter, MAP range: range of mean annual precipitation, CCV_MN: mean climate-change velocity, AAC: availability of analogous climates, PS: precipitation seasonality, MDR: mean diurnal range, ALT: altitude, HL: habitat loss, HFP: human footprints, RL: road length, POP: population density, SHEI: Shannon's evenness index, CAI_MN: mean core area index, CAI_CV: coefficient of variance of core area index.

(152,500 km^2), accounting for 64.2% of the total 95 TSR hotspot cells (237,500 km^2). When the criterion was relaxed to 5% upper quantile for SR (and TSR) and $P < 0.05$ significance level for RER, 72 cells (180,000 km^2) are found overlapped between the RER and SR hotspots, accounting for 39.8% of RER hotspot cells (Fig. 2B), but 72.9% of TSR hotspot cells were overlapped with SR hotspots in this case (Fig. 2B).

The difference between TSR and RER defined risks can be further illustrated by the following results. Area 1 (southeast Tibet), area 2 (Hengduan Mountains), and area 3 (Xishuangbanna Region) in Fig. 1C were identified as biodiversity hotspots by total species richness (Fig. 1A; there were 3441, 5475 and 3486 species, respectively) and threat hotspots by TSR (Fig. 1B; 225, 691, and 635, respectively). By the measure of RER, area 1 and 3 were also identified as hotspots at the $P < 0.01$ significance level but area 2 was identified as marginally significant ($P < 0.05$) (Fig. 1C). In contrast, areas 4 (Sichuan Basin), 5 (Guangdong Hills), and 6 (Northeast Plain) were not identified as biodiversity or threatened species richness hotspots (SR and TSR were below the criterion of 5% upper quantile; Fig. 1A and B), but these three areas were identified as RER hotspots (due to their high proportions of threatened species, 127/1104, 130/1691, and 14/415, respectively).

The distributions of both TSR and RER can be well explained by environmental and human activity variables. As shown by the "best" models selected by the AIC in Table 1, the models for threatened species richness and relative extinction risk shared many common environmental and human activity variables but also differed in many of them. Specifically, environmental effects on TSR and RER include energy and water availability, topographic heterogeneity, and climatic variability/stability factors (Table 1). Among those environmental variables that were different between the two models, altitude (ALT) had no significant effect on TSR while the standard deviation of altitude (ALT_STD) was only selected by the RER model.

The most interesting difference between the TSR and RER models is reflected in the effects of human activity variables (Table 1). Among the three major anthropogenic factors (habitat loss, land use intensity, and habitat fragmentation), habitat loss (HL) showed a negative effect on TSR but its effect on RER was quadratic. The quadratic term of population density (POP) was significantly negative on TSR but not on RER. Road length (RL) was only selected by the RER model. Habitat fragmentation (CAI_MN) showed no significant effect on TSR but a highly significant effect on RER. Although all the interaction terms in the TSR model were significant, only one of them was significant in the RER model (Table 1).

We also found that RER was a better indicator of ecosystem functioning loss, as measured by relative temporal change of NPP, than TSR (Fig. 3). The relationship between NPP and SR (or TSR) was less consistent. For example, between 2000 and 2015, NPP decreased in RER hotspots where SR and TSR were low (such as areas 4, 5, and 6) but increased in some SR and TSR hotspots where RER was low (around area 2).

5. Discussion

Biodiversity mapping is a major tool for biodiversity study and conservation. It is particularly useful for describing biodiversity patterns and monitoring conservation status (Jenkins et al., 2013; Watson et al., 2013). Although conservation planning is encouraged to use methods that can directly incorporate threats, such as Marxan and C-plan (Watts et al., 2017), to identify priority areas, threatened species richness remains the essential biodiversity measure in such exercises. The conventional approach maps the absolute richness of threatened or endemic species and measures the magnitude of extinction risk as well as irreplaceability in an area. Our results confirmed that the threatened species richness (Fig. 1B) and the total species richness (Fig. 1A) were highly congruent, with over 60% of variation in TSR being explained by SR.

With little doubt, areas with both high threat and high number of species should be considered as the priorities in conservation practice. For example, the Xishuangbanna region (area 3 as identified in Fig. 1C) was identified as a hotspot in terms of SR and TSR (Fig. 1A, B). Xishuangbanna lies within the Indo-Burma global biodiversity hotspot and harbors some 16% of the vascular flora of China (Zhang and Cao, 1995). The area has suffered substantial deforestation and land use change with much of the primary tropical forests being converted to rubber plantation or other developments (Xu et al., 2014).

TSR measures the *magnitude* of the threat to diversity in an area and conservation actions based on the absolute threatened or endemic species richness could be proactive in the long term. In contrast, RER measures the *degree* of threat an area has suffered and thus is complementary to TSR. The RER is particularly useful for identifying areas with considerable threats but low diversity (Brooks et al., 2006; Turner et al., 2007). This was also evident in our study. For instance, the populous southern and northeastern China (areas 4, 5 and 6, see Fig. 1C) were major RER hotspots suffering a high degree of extinction risk, but they are not SR hotspots (Fig. 1A) nor TSR hotspots (Fig. 1B). This shows how non-SR or TSR hotspots could be disproportionally affected by human activities; common to these three areas is that they are highly populated (e.g., the present population density is 530 people/km^2 in

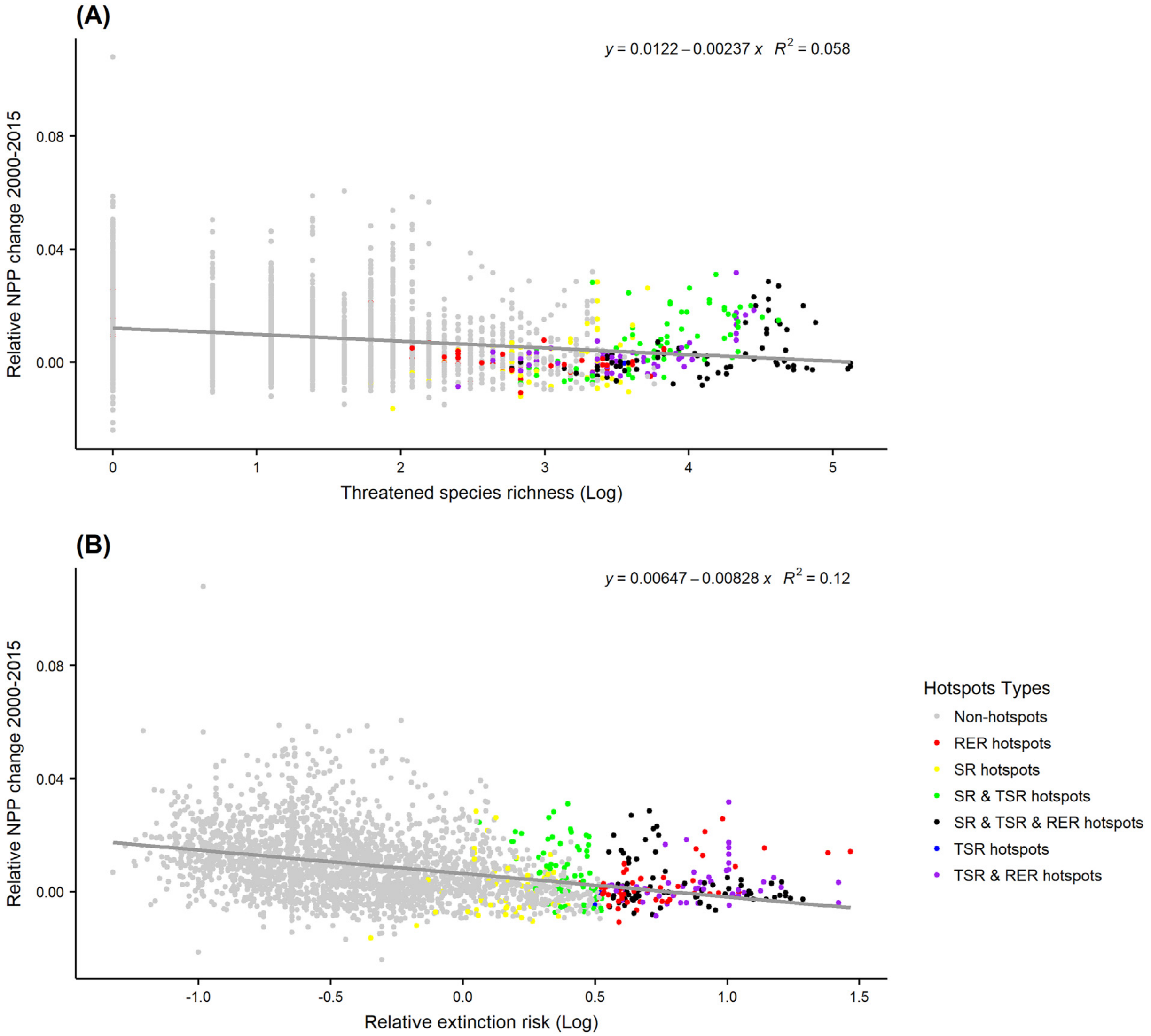

Fig. 3. Relationships between (A) threatened species richness (TSR) ($R^2 = 0.058$, $P < 0.001$), (B) relative extinction risk (RER) ($R^2 = 0.12$, $P < 0.001$) and relative temporal change of net primary productivity (NPP) from 2000 to 2015 (calculated as temporal NPP change divided by the NPP in year 2000). Primary color dots indicate grid cells unique to one type of hotspot (yellow, species richness ranked top 5%; blue, threatened species richness ranked top 5%; red, relative extinction risk at the significance level $P < 0.05$), secondary color dots indicate overlap between two types, and black indicates overlap of all three types. (For interpretation of the references to color in this figure legend, the reader is referred to the web version of this article.)

area 4, Sichuan Basin) and have long histories of cultivation (d'Alpoim Guedes, 2011; He et al., 2014; Feng et al., 2017). In contrast, the Hengduan Mountains (area 2), a global biodiversity hotspot (Myers et al., 2000) with many endemic and threatened species, was identified as a SR and TSR hotspot (Fig. 1A, B). However, the area has suffered relatively low human activities because of its inaccessibility and low human population density (~3 people/km^2). This area was identified as a less significant hotspot ($P < 0.05$) by RER (Fig. 1C), indicating that the degree of threat is not as serious as for areas 4, 5, and 6. These results suggest that it would be cost-effective to conserve the Hengduan Mountains area (because of its high TSR) but if resources are limited, the area should be of relatively low priority for conservation investment because of its low degree of threats (low RER) compared to areas 4, 5, and 6. It is clear that RER, being complementary to TSR, can contribute to identifying potential gaps of the TSR or SR based conservation planning systems.

Conservation is ultimately about maintaining biodiversity by minimizing and averting the impacts of multiple threatening factors. If the final goal is to reduce the direct pressures on biodiversity and to safeguard ecosystems as well as species diversity (e.g., Convention on Biological Diversity Aichi Targets 6 & 12), it is essential to identify underlying threat processes occurring within an area, whether the area is species-rich or species-poor. The regression model of RER (Eq. (14)) allows us to do so. Although many of the RER-identified risk factors also affect TSR (Table 1), there is no methodological or ecological reason that this has to be the case. A high TSR could arise from a high total species richness (i.e., by chance alone a high SR could lead to a high TSR) or high threats, or both, in an area. As such, it is ambivalent to use a TSR hotspot to infer underlying causes. After the effect of the total number of species has been accounted for, our results show that TSR and RER of the angiosperm species in China are affected by many shared environmental factors but different human activity factors at both the 50 km (Table 1) and the 100 km scale (Appendix Table S2). Among the differences between TSR and RER models, the significant environmental covariates selected by the RER model (Table 1) suggest that threatened species are particularly vulnerable in areas at low altitude (ALT) but with a high degree of topographic heterogeneity (ALT_STD). The effects of historical climate change and the availability of analogous distribution area (CCV_MN, AAC and CCV_STD) on RER are important at the 50 km scale (Table 1) but not at the 100 km scale

(Appendix Table S2). The most significant environmental covariates in the TSR regression model are energy and water availability and climatic variability (PET, MI, CCV_MN and PS), suggesting the importance of energy and water in determining species richness or endemism as well as extinction risk (Kreft and Jetz, 2007; Sandel et al., 2011). The consistency in environmental effects on RER and TSR highlights the “irreplaceable” aspect of physical environments as “arenas” for biological activity (Beier and Brost, 2010). However, the “vulnerability” aspect of extinction risk was better revealed by RER from the effects of habitat loss and road length. The human footprint (HFP) had a significantly positive effect on both TSR and RER, but the effect of habitat loss was significantly negative (Table 1). This is not unexpected given that our measure of habitat loss mainly reflects historical area loss of natural habitat in China from the 1950s to the 1980s (Appendix Table S2 and Table 1) while human footprint indicates current intensity of human activities. Although habitat loss and fragmentation metrics (e.g., SHEI and CAI_MN) could impose joint threats to many species (Mantyka-pringle et al., 2012), none of the interactions in our study were significant (Tables 1 and S2). This is possibly because the effect of habitat loss was so strong that it overwhelmed the effect of fragmentation, consistent with the "habitat amount hypothesis" (Fahrig, 2013). To investigate that, we conducted an analysis by purposely excluding the habitat loss terms (i.e., HL and HL^2) from the RER regression model but retaining the HL interaction terms (see Table 1). This analysis showed that the HL interaction terms had highly significant effects on RER (results not shown).

It is necessary to mention a caveat for our study. IUCN endangered species were identified by criteria relating to population size, range size, population decline, and habitat fragmentation. Although the detailed factors used to classify China 2013 Red List species are unknown, there is a possibility that the factors used to define an endangered species are also used as covariates in our regression models. This could unintentionally elevate the importance of such covariates as risk factors. This inflation could potentially contribute to the significant correlation observed between TSR and habitat fragmentation metrics, although this still cannot explain the negative effect of habitat loss on TSR.

Having understood the distinction between TSR and RER (the former measures the absolute risk, the latter measures the degree of extinction risk), the question naturally arises as to which of the two measures better indicates the degradation of ecosystem functioning. Although both TSR and RER are significantly correlated with the decreasing trend of NPP from 2000 to 2015, RER is clearly more strongly associated with the degradation of ecosystem functioning (Fig. 3). The oft-documented positive relationship between biodiversity and ecosystem functioning (Bunker et al., 2005) predicts that loss of species from local communities could result in loss of biological insurance and species-poor communities would suffer more from losing the same number of species. As such, RER should be a better indicator of the change of ecosystem functioning, including climate change mitigation such as change in NPP.

To summarize, we have proposed a novel approach for biodiversity mapping and demonstrated its application to mapping and analyzing the extinction risk of angiosperm species in China. The basic concept of the method is relative extinction risk (RER) that describes the degree species suffer from threats. In contrast to the conventionally used absolute number of threatened species, RER removes the confounding effect of background species richness. There is a well-developed theory about RER in epidemiology that allows for a formal statistical definition of “RER hotspots” as well as a prediction tool (Waller and Carlin, 2010). RER mapping provides an alternative description of the extinction risk distribution of threatened species that better indicates degeneration of ecosystem functioning. If used together with species-specific evaluation on extinction risk, such as the IUCN Red List, RER mapping should complement conventional conservation methods to facilitate biodiversity conservation and management.

Supplementary data to this article can be found online at https://doi.org/10.1016/j.biocon.2018.07.012.

References

Ahn, C.-H., Tateishi, R., 1994. Development of a global 30-minute grid potential evapotranspiration data set. J. Jpn. Soc. Photogramm. Remote Sensing 33, 12–21.

Beier, P., Brost, B., 2010. Use of land facets to plan for climate change: conserving the arenas, not the actors. Conserv. Biol. 24, 701–710.

Brooks, T.M., Mittermeier, R.A., Mittermeier, C.G., Da Fonseca, G.A.B., Rylands, A.B., Konstant, W.R., Flick, P., Pilgrim, J., Oldfield, S., Magin, G., Hilton-Taylor, C., 2002. Habitat loss and extinction in the hotspots of biodiversity. Conserv. Biol. 16, 909–923.

Brooks, T.M., Mittermeier, R.A., da Fonseca, G.A.B., Gerlach, J., Hoffmann, M., Lamoreux, J.F., Mittermeier, C.G., Pilgrim, J.D., Rodrigues, A.S.L., 2006. Global biodiversity conservation priorities. Science 313, 58–61.

Bunker, D.E., DeClerck, F., Bradford, J.C., Colwell, R.K., Perfecto, I., Phillips, O.L., Sankaran, M., Naeem, S., 2005. Species loss and aboveground carbon storage in a tropical forest. Science 310, 1029–1031.

Canadell, J.G., Raupach, M.R., 2008. Managing forests for climate change mitigation. Science 320, 1456–1457.

Ceballos, G., Ehrlich, P.R., 2006. Global mammal distributions, biodiversity hotspots, and conservation. Proc. Natl. Acad. Sci. 103, 19374–19379.

Clayton, D., Kaldor, J., 1987. Empirical bayes estimates of age-standardized relative risks for use in disease mapping. Biometrics 43, 671–681.

d'Alpoim Guedes, J., 2011. Millets, rice, social complexity, and the spread of agriculture to the Chengdu Plain and Southwest China. Rice 4, 104–113.

Davies, R.G., Orme, C.D.L., Olson, V., Thomas, G.H., Ross, S.G., Ding, T.-S., Rasmussen, P.C., Stattersfield, A.J., Bennett, P.M., Blackburn, T.M., Owens, I.P.F., Gaston, K.J., 2006. Human impacts and the global distribution of extinction risk. Proc. R. Soc. B Biol. Sci. 273, 2127–2133.

Devine, O.J., Louis, T.A., Halloran, M.E., 1996. Identifying areas with elevated disease incidence rates using empirical Bayes estimators. Geogr. Anal. 28, 187–199.

Di Marco, M., Rondinini, C., Boitani, L., Murray, K.A., 2013. Comparing multiple species distribution proxies and different quantifications of the human footprint map, implications for conservation. Biol. Conserv. 165, 203–211.

Elliott, P., Wartenberg, D., 2004. Spatial epidemiology: current approaches and future challenges. Environ. Health Perspect. 112, 998–1006.

Fahrig, L., 2003. Effects of habitat fragmentation on biodiversity. Annu. Rev. Ecol. Evol. Syst. 34, 487–515.

Fahrig, L., 2013. Rethinking patch size and isolation effects: the habitat amount hypothesis. J. Biogeogr. 40, 1649–1663.

Feng, G., Mao, L., Benito, B.M., Swenson, N.G., Svenning, J.-C., 2017. Historical anthropogenic footprints in the distribution of threatened plants in China. Biol. Conserv. 210, 3–8.

Grenyer, R., Orme, C.D.L., Jackson, S.F., Thomas, G.H., Davies, R.G., Davies, T.J., Jones, K.E., Olson, V.A., Ridgely, R.S., Rasmussen, P.C., Ding, T.-S., Bennett, P.M., Blackburn, T.M., Gaston, K.J., Gittleman, J.L., Owens, I.P.F., 2006. Global distribution and conservation of rare and threatened vertebrates. Nature 444, 93–96.

Griffith, D.A., 2003. Spatial Autocorrelation and Spatial Filtering: Gaining Understanding Through Theory and Scientific Visualization. Springer Science & Business Media.

Griffith, D.A., Peres-Neto, P.R., 2006. Spatial modeling in ecology: the flexibility of eigenfunction spatial analyses. Ecology 87, 2603–2613.

Hansen, M.C., Potapov, P.V., Moore, R., Hancher, M., Turubanova, S.A., Tyukavina, A., Thau, D., Stehman, S.V., Goetz, S.J., Loveland, T.R., Kommareddy, A., Egorov, A., Chini, L., Justice, C.O., Townshend, J.R.G., 2013. High-resolution global maps of 21st-century forest cover change. Science 342, 850–853.

He, F., 2009. Price of prosperity: economic development and biological conservation in China. J. Appl. Ecol. 46, 511–515.

He, C., Liu, Z., Tian, J., Ma, Q., 2014. Urban expansion dynamics and natural habitat loss in China: a multi-scale landscape perspective. Glob. Chang. Biol. 20, 2886–2902.

Hijmans, R.J., Cameron, S.E., Parra, J.L., Jones, P.G., Jarvis, A., 2005. Very high resolution interpolated climate surfaces for global land areas. Int. J. Climatol. 25, 1965–1978.

Hooper, D.U., Adair, E.C., Cardinale, B.J., Byrnes, J.E.K., Hungate, B.A., Matulich, K.L., Gonzalez, A., Duffy, J.E., Gamfeldt, L., O'Connor, M.I., 2012. A global synthesis reveals biodiversity loss as a major driver of ecosystem change. Nature 486, 105–108.

IUCN, 2001. IUCN Red List Categories and Criteria: Version 3.1. IUCN, Gland, Switzerland and Cambridge, UK.

Jenkins, C.N., Pimm, S.L., Joppa, L.N., 2013. Global patterns of terrestrial vertebrate diversity and conservation. Proc. Natl. Acad. Sci. 110, E2602–E2610.

Kreft, H., Jetz, W., 2007. Global patterns and determinants of vascular plant diversity. Proc. Natl. Acad. Sci. 104, 5925–5930.

Lawson, A.B., 2013. Statistical Methods in Spatial Epidemiology. John Wiley & Sons.

Lee, T.M., Jetz, W., 2011. Unravelling the structure of species extinction risk for predictive conservation science. Proc. R. Soc. B Biol. Sci. 278, 1329–1338.

Lennon, J.J., Koleff, P., Greenwood, J.J.D., Gaston, K.J., 2004. Contribution of rarity and commonness to patterns of species richness. Ecol. Lett. 7, 81–87.

Mantyka-pringle, C.S., Martin, T.G., Rhodes, J.R., 2012. Interactions between climate and habitat loss effects on biodiversity: a systematic review and meta-analysis. Glob. Chang. Biol. 18, 1239–1252.

Margules, C.R., Pressey, R.L., 2000. Systematic conservation planning. Nature 405, 243–253.

McGarigal, K., Cushman, S., Ene, E., 2012. FRAGSTATS v4: Spatial Pattern Analysis

Program for Categorical and Continuous Maps. University of Massachusetts, Amherst (Computer software program produced by the authors at the University of Massachusetts).

Myers, N., Mittermeier, R.A., Mittermeier, C.G., da Fonseca, G.A.B., Kent, J., 2000. Biodiversity hotspots for conservation priorities. Nature 403, 853–858.

Ohlemüller, R., Anderson, B.J., Araújo, M.B., Butchart, S.H.M., Kudrna, O., Ridgely, R.S., Thomas, C.D., 2008. The coincidence of climatic and species rarity: high risk to small-range species from climate change. Biol. Lett. 4, 568–572.

Orme, C.D.L., Davies, R.G., Burgess, M., Eigenbrod, F., Pickup, N., Olson, V.A., Webster, A.J., Ding, T.-S., Rasmussen, P.C., Ridgely, R.S., Stattersfield, A.J., Bennett, P.M., Blackburn, T.M., Gaston, K.J., Owens, I.P.F., 2005. Global hotspots of species richness are not congruent with endemism or threat. Nature 436, 1016–1019.

Pimm, S.L., Jenkins, C.N., Abell, R., Brooks, T.M., Gittleman, J.L., Joppa, L.N., Raven, P.H., Roberts, C.M., Sexton, J.O., 2014. The biodiversity of species and their rates of extinction, distribution, and protection. Science 344, 1246752.

Prentice, R.L., 1985. Relative risk regression analysis of epidemiologic data. Environ. Health Perspect. 63, 225–234.

Ran, Y., Li, X., Lu, L., 2010. Evaluation of four remote sensing based land cover products over China. Int. J. Remote Sens. 31, 391–401.

Ricklefs, R.E., He, F., 2016. Region effects influence local tree species diversity. Proc. Natl. Acad. Sci. 113, 674–679.

Rosenzweig, M.L., 1995. Species Diversity in Space and Time. Cambridge University Press.

Saint-Jacques, N., Lee, J.S.W., Brown, P., Stafford, J., Parker, L., Dummer, T.J.B., 2016. Small-area spatio-temporal analyses of bladder and kidney cancer risk in Nova Scotia, Canada. BMC Public Health 16, 175.

Sandel, B., Arge, L., Dalsgaard, B., Davies, R.G., Gaston, K.J., Sutherland, W.J., Svenning, J.-C., 2011. The influence of late Quaternary climate-change velocity on species endemism. Science 334, 660–664.

Sartorius, B.K.D., Sartorius, K., Chirwa, T.F., Fonn, S., 2011. Infant mortality in South Africa—distribution, associations and policy implications, 2007: an ecological spatial analysis. Int. J. Health Geogr. 61.

Sartorius, B., Cohen, C., Chirwa, T., Ntshoe, G., Puren, A., Hofman, K., 2013. Identifying high-risk areas for sporadic measles outbreaks: lessons from South Africa. Bull. World Health Organ. 91, 174–183.

Shacham, E., Nelson, E.J., Hoft, D.F., Schootman, M., Garza, A., 2017. Potential high-risk areas for Zika virus transmission in the contiguous United States. Am. J. Public Health 107, 724–731.

Shafer, S.L., Bartlein, P.J., Thompson, R.S., 2001. Potential changes in the distributions of western North America tree and shrub taxa under future climate scenarios. Ecosystems 4, 200–215.

Shearer, F.M., Longbottom, J., Browne, A.J., Pigott, D.M., Brady, O.J., Kraemer, M.U.G., Marinho, F., Yactayo, S., de Araújo, V.E.M., da Nóbrega, A.A., Fullman, N., Ray, S.E., Mosser, J.F., Stanaway, J.D., Lim, S.S., Reiner Jr., R.C., Moyes, C.L., Hay, S.I., Golding, N., 2018. Existing and potential infection risk zones of yellow fever worldwide: a modelling analysis. Lancet Glob. Health 6, e270–e278.

Turner, W.R., Brandon, K., Brooks, T.M., Costanza, R., da Fonseca, G.A.B., Portela, R., 2007. Global conservation of biodiversity and ecosystem services. Bioscience 57, 868–873.

Venter, O., Sanderson, E.W., Magrach, A., Allan, J.R., Beher, J., Jones, K.R., Possingham, H.P., Laurance, W.F., Wood, P., Fekete, B.M., Levy, M.A., Watson, J.E.M., 2016. Global terrestrial human footprint maps for 1993 and 2009. Sci. Data 3, 160067.

Wakefield, J., 2007. Disease mapping and spatial regression with count data. Biostatistics 8, 158–183.

Waller, L.A., Carlin, B.P., 2010. Disease mapping. In: Chapman & Hall/CRC Handbooks of Modern Statistical Methods, pp. 217–243 (2010).

Wang, X., Blanchet, F.G., Koper, N., 2014. Measuring habitat fragmentation: an evaluation of landscape pattern metrics. Methods Ecol. Evol. 5, 634–646.

Watson, J.E.M., Iwamura, T., Butt, N., 2013. Mapping vulnerability and conservation adaptation strategies under climate change. Nat. Clim. Chang. 3, 989–994.

Watts, M.E., Stewart, R.R., Martin, T.G., Klein, C.J., Carwardine, J., Possingham, H.P., 2017. Systematic conservation planning with Marxan. In: Gergel, S.E., Turner, M.G. (Eds.), Learning Landscape Ecology: A Practical Guide to Concepts and Techniques. Springer New York, New York, NY, pp. 211–227.

Xu, J., Grumbine, R.E., Beckschäfer, P., 2014. Landscape transformation through the use of ecological and socioeconomic indicators in Xishuangbanna, Southwest China, Mekong Region. Ecol. Indic. 36, 749–756.

Yang, W., Ma, K., Kreft, H., 2013. Geographical sampling bias in a large distributional database and its effects on species richness–environment models. J. Biogeogr. 40, 1415–1426.

Zhang, J., Cao, M., 1995. Tropical forest vegetation of Xishuangbanna, SW China and its secondary changes, with special reference to some problems in local nature conservation. Biol. Conserv. 73, 229–238.

Zhao, M., Running, S.W., 2010. Drought-induced reduction in global terrestrial net primary production from 2000 through 2009. Science 329, 940–943.